ACS MEASUREMENT SCIENCE Au
AN OPEN ACCESS JOURNAL OF THE AMERICAN CHEMICAL SOCIETY

pubs.acs.org/measureau

Letter

Mixed-Metal-Atom Markers Enable Simultaneous Imaging of Spatial Distribution in Two-Dimensional Heterogeneous Molecular Assembly by Scanning Transmission Electron Microscopy

Ikumi Akita, Yohei Ishida,* and Tetsu Yonezawa*

Cite This: *ACS Meas. Sci. Au* 2022, 2, 542−546

Read Online

ACCESS | Metrics & More | Article Recommendations | Supporting Information

ABSTRACT: Atomic-scale observation by aberration-corrected scanning transmission electron microscopy (STEM) is essential for characterizing supramolecular assemblies with nonperiodic structures. Identifying the relative spatial arrangement in a mixture of molecular species in an assembly is crucial for understanding chemical reaction systems occurring in the assembly. Herein, we report the first direct observation of supramolecular assemblies comprising anionic clay mineral nanosheets and two types of cationic porphyrin complexes with Pt and Pd atom markers by annular dark-field STEM, enabling the simultaneous imaging of well-mixed spatial molecular distributions. The results expand the possibility of applying electron microscopy to self-assembly structures constructed via weak supramolecular interactions on relatively thick nanosheet materials and on one- to few-atom-thick graphene analogues, which will provide important guidelines for future material design.

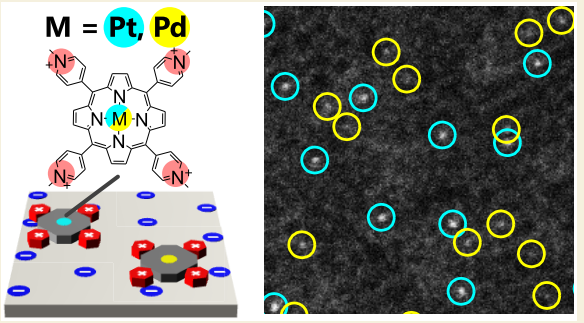

KEYWORDS: *Scanning Transmission Electron Microscopy, Electrostatic Interaction, Supramolecules, Clay Minerals, Nanosheet, 2D Material*

Atomic-scale observation by aberration-corrected (scanning) transmission electron microscopy ((S)TEM) is essential for the characterization of nanomaterials with nonperiodic structures, such as supramolecular assemblies comprising organic molecules and inorganic substrates.[1−6] Understanding the behavior of molecules in nonperiodic supramolecular assemblies at the molecular scale, such as intermolecular distance, orientation, and molecular structural changes, is essential for a deeper understanding and control of the functions of materials. Beyond the averaged structural information generally obtained by spectroscopic, crystallographic, and nuclear magnetic resonance (NMR) techniques,[7−11] the direct imaging of individual molecules in supramolecular assemblies provides important guidelines for designing nanomaterials.

Recently, we successfully demonstrated the first annular dark-field (ADF) STEM observation of an assembly of organic molecules on monolayer montmorillonite-type clay mineral nanosheets anchored via multiple electrostatic interactions using Pt-coordinated porphyrin complexes, where the Pt atom worked as a marker.[12] Montmorillonite, a typical clay mineral, is layered aluminosilicate with atomically flat surfaces and high surface charge densities in which Mg^{2+} is isomorphically substituted with Al^{3+} in the octahedral layer (Figure 1, right panel), which generates a Coulombic field to form stable complexes with cationic molecules.[7−10] The key factor for the

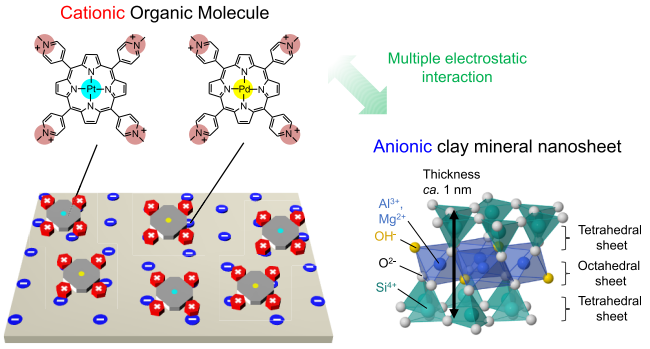

Figure 1. Schematic of a supramolecular assembly based on multiple electrostatic interactions between the anionic clay mineral nanosheet and two types of cationic metalloporphyrins (left) and cross-sectional image of the unit structure of the monolayer clay mineral nanosheet (right, montmorillonite).

Received: June 22, 2022
Revised: July 28, 2022
Accepted: August 1, 2022
Published: August 3, 2022

https://doi.org/10.1021/acsmeasuresciau.2c00043
ACS Meas. Sci. Au 2022, 2, 542−546

stable observation of individual organic molecules in a supramolecular assembly is the strong fixation of molecules via multiple electrostatic interactions, which allows for the determination of the relative spatial arrangement of the molecules. Because the ADF-STEM contrast is proportional to the 1.4th−2nd power of the atomic number (Z-contrast),[13] various molecules should be simultaneously identifiable using a series of markers with different atomic numbers. The assembly of various molecules is a decisive idea in designing intermolecular chemical reactions, on-surface organic synthesis, and photochemical energy or electron transfers.[7,8,10,11,14]

Therefore, identifying the relative arrangement of heterogeneous molecules in an assembly is crucial for a detailed understanding of the functions and chemical reactions occurring in the assembly (see the common distribution models in Figure S1 in the Supporting Information).[7,15,16] Herein, we demonstrate the first direct observation of a well-mixed spatial molecular distribution of two types of porphyrin complexes with Pt and Pd atom markers on relatively thick monolayer clay mineral nanosheet strongly anchored via multiple electrostatic interactions.

Figure 1 illustrates the structure of the Pt+PdTMPyP-clay mineral nanosheet assembly. It was prepared by mixing the aqueous dispersion of clay mineral nanosheets and two types of tetrakis(1-methylpyridinium-4-yl) porphyrins coordinated with Pt (PtTMPyP) and Pd (PdTMPyP) in a ratio of 1:1 (mol/mol), denoted as Pt+PdTMPyP. Both Pt- and Pd-porphyrin complexes have four cationic substituents in their structures and thus form stable complexes with clay mineral nanosheets via multiple electrostatic interactions. The monomeric adsorption of Pt+PdTMPyP on the clay mineral nanosheets was confirmed by the absorption spectra of Pt+PdTMPyP-, PtTMPyP-, and PdTMPyP-clay (Figure 2). The concentration

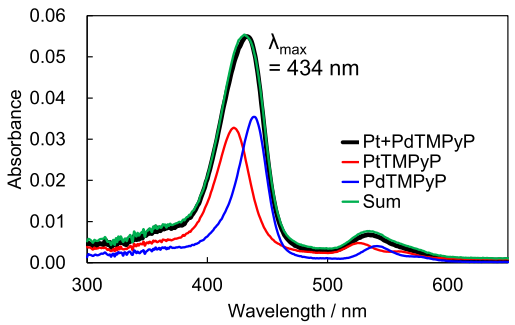

Figure 2. Absorption spectra of Pt+PdTMPyP (black), PtTMPyP (red), and PdTMPyP (blue) on clay mineral nanosheet and the sum of the spectra of PtTMPyP and PdTMPyP (green). Dye loading of PtTMPyP and PdTMPyP was 45% CEC of clay.

of molecules on the clay mineral nanosheets was expressed as the loading level vs cation exchange capacity (CEC) of the clay, which is the ratio between the amount of cation charge of the molecule and the CEC of the clay mineral nanosheet. The saturated concentration of monomeric adsorption of both PtTMPyP-clay and PdTMPyP-clay was determined to be 90% (Figure S2). The absorption spectrum of the mixed sample (Pt+PdTMPyP-clay) can be fitted by the sum of the individual absorption spectra of PtTMPyP-clay and PdTMPyP-clay (Figure 2), indicating that both molecules adsorb monomerically on the clay mineral nanosheet, even in the mixed sample. Further, the constant spectral features of the 45 and 90% samples indicate monomeric adsorption even under dense 90% conditions (Figure S3). ADF-STEM observations were conducted on a sample with a saturated molecular concentration of 90%, which had a uniform density. Note that the maximum absorption wavelength shifted to a longer wavelength upon adsorption on the clay mineral nanosheet (Figures S2 and S3) because of the planarization of the methylpyridinium substituent with respect to the porphyrin core, as reported elsewhere.[8]

Before the ADF-STEM measurements, a multislice ADF-STEM image simulation was performed to evaluate the difference in ADF-STEM contrast between Pt and Pd markers on clay mineral nanosheets. An atomic model of Pt+PdTMPyP-clay (Figure 3a) was constructed to ensure that

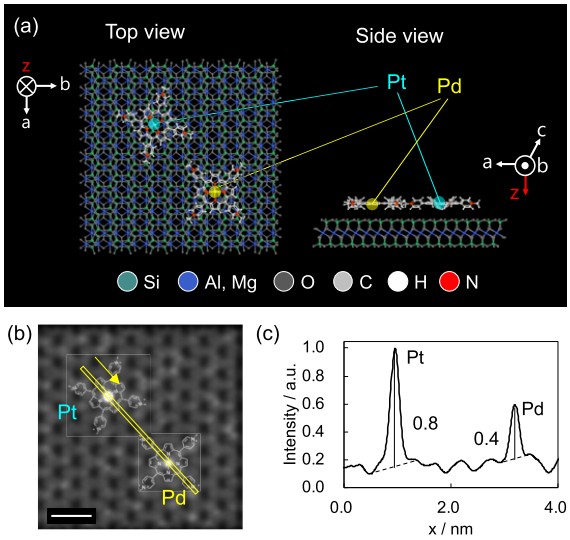

Figure 3. (a) Atomic models of PtTMPyP and PdTMPyP on a monolayer clay mineral nanosheet, (b) corresponding simulated ADF-STEM image, and (c) intensity profile of the yellow boxed region in (b). Scale bar = 1 nm. Hydrogen atoms in clay mineral nanosheets are omitted for clarity.

the nitrogen atoms of the methylpyridinium substitutes of the molecule and the oxygen atoms on the surface of the clay mineral nanosheets were in the closest proximity considering their van der Waals radii. The dihedral angle between the porphyrin core and methylpyridinium substituents was set to 42°, as described in our previous study.[12] ADF imaging is considered an incoherent imaging, wherein the ADF-detected emission intensities from scattered electrons can be quantitatively analyzed as the integral of the intensities scattered by each atom. When the inner semiangle of the ADF detector is sufficiently large, scattering by the nuclear potential becomes dominant and the effect of coherent scattering can be almost ignored. Therefore, the thermal diffusion scattering (i.e., Rutherford scattering) becomes dominant, and the ADF signal is then proportional to the 1.4th−2nd power of the atomic number Z.[13] Under this assumption, which is applicable to the current work (see the experimental details and calculation conditions in the Supporting Information), the simulated ADF-STEM image of Pt+PdTMPyP-clay in Figure 3b shows that both Pt and Pd markers can be visualized on clay mineral nanosheets with distinct differences in their intensities (see the same simulation image without annotations in Figure S4). The intensity profile of the yellow boxed region in Figure 3b

https://doi.org/10.1021/acsmeasuresciau.2c00043
ACS Meas. Sci. Au 2022, 2, 542−546

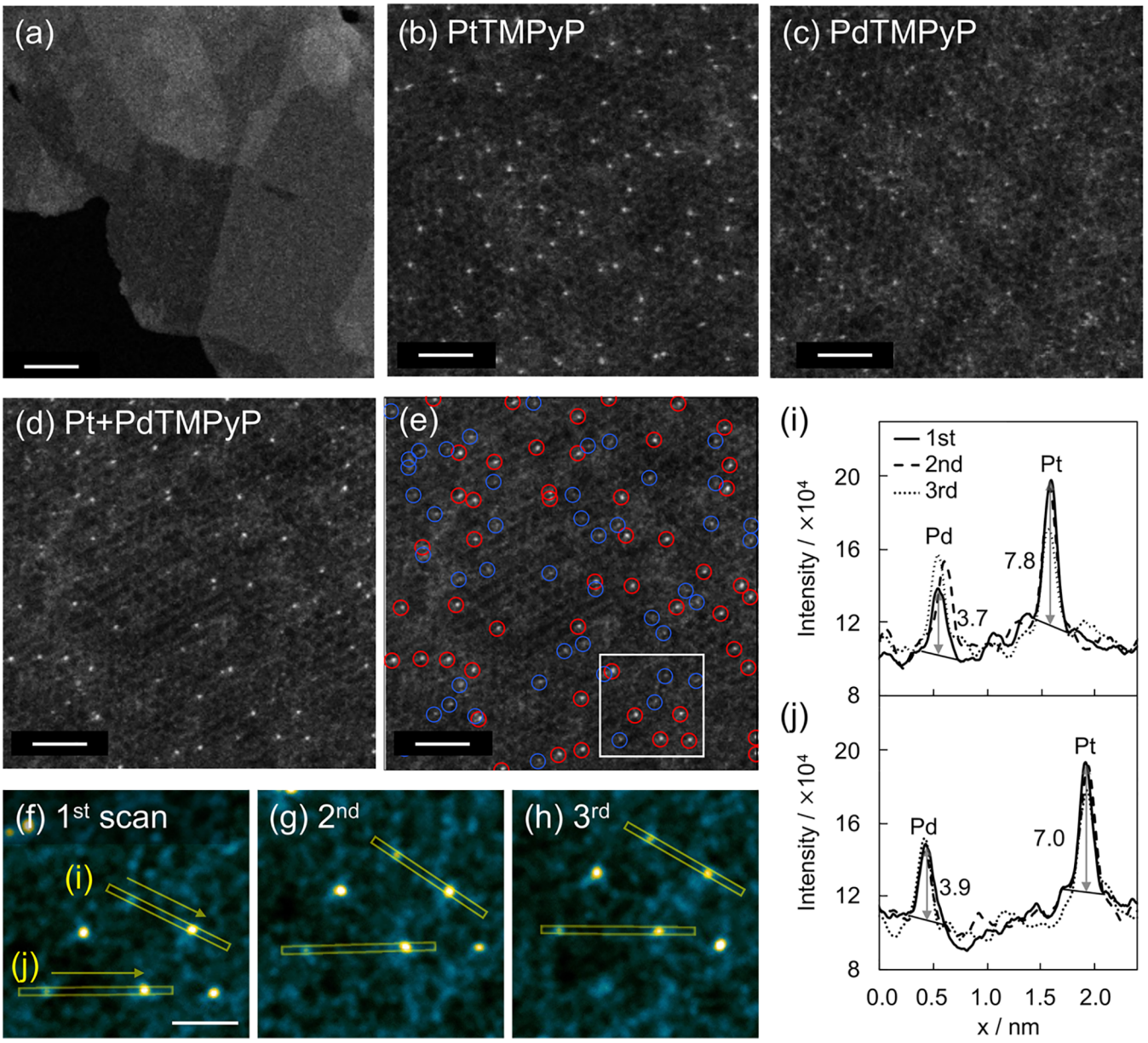

Figure 4. Experimental ADF-STEM images of (a) pristine clay mineral nanosheet at low magnification and (b) PtTMPyP-, (c) PdTMPyP-, and (d) Pt+PdTMPyP-clay at dye loadings of 90% vs CEC of clay. (e) Distribution of Pt and Pd markers in (d) indicated by red and blue circles, respectively. (f–h) Enlarged images of the white boxed region in (e) obtained by repeated scanning from the first to the third scan. (i,j) Corresponding intensity profiles of the yellow boxed regions in (f) of first (solid), second (dashed), and third (dotted line) scans. Scale bar = 50 nm for (a), 2 nm for (b–e), and 1 nm for (f–h).

indicates the intensity ratio between the Pt and Pd markers is approximately 2 (Figure 3c). Thus, Pt and Pd atom markers can be intuitively identified by the difference in the ADF-STEM contrast.

Figure 4 shows the results of the ADF-STEM observations at the acceleration voltage of 80 kV for the PtTMPyP-, PdTMPyP-, and Pt+PdTMPyP-clay assemblies (see the details of imaging parameters in experimental section in the Supporting Information). The ADF conditions were set for the following reasons: (1) the crystal structure of the clay mineral nanosheet remained intact during several repeated scannings; (2) the periodical contrast of the clay mineral nanosheet and bright contrast of metal atoms were stably observable without significant streaking. As shown in the low-magnification image of the pristine clay mineral nanosheet in Figure 4a, the sample was deposited horizontally on the pores of the lacy carbon film. The monolayer region was determined by the difference in contrast. High-magnification ADF-STEM images of PtTMPyP- and PdTMPyP-clay (Figure 4b,c) show apparent bright spots corresponding to Pt and Pd markers and periodic contrast of the clay mineral nanosheet (also see Figure S5a).[17] The bright spots were not found to segregate to the edges, interior, or interlayers of the clay mineral nanosheet, indicating that the molecules were uniformly adsorbed and were well-dispersed on the nanosheet surface. The Zn-coordinated counterpart showed no apparent bright spots, and the contrast was similar to that of the pristine clay mineral nanosheet (Figure S5b). Therefore, an element with an atomic number smaller than Zn (Z = 30) is not suitable as an ADF-STEM marker on relatively thick clay mineral nanosheets.

https://doi.org/10.1021/acsmeasuresciau.2c00043
ACS Meas. Sci. Au 2022, 2, 542–546

Although various elements, even those with small atomic numbers such as Cu ($Z = 29$),[18] have been reported to be used as markers in ADF observations for one- or few-atom-thick materials such as graphene[18−22] and monolayer MoS_2,[23] clay mineral nanosheets with a relatively complex unit layer structure limit low-contrast observations.

The experimental ADF-STEM image of the Pt+PdTMPyP90%-clay assemblies in Figure 4d shows bright spots with two different levels of intensity, which are considered to be Pt and Pd markers, respectively. The intensity histogram of bright spots in Pt+PdTMPyP-clay in Figure S6a exhibits a bimodal distribution, where the two peaks are considered to be Pt and Pd atoms, and their counts are approximately the same. According to the classification obtained from the histogram, the well-mixed distributions of PtTMPyP (red) and PdTMPyP (blue) were visualized at the atomic scale for the first time, as shown in Figure 4e. A Pt/Pd ratio of approximately 1:1 was observed in every region of the image, for example, 6×6 nm^2, including ∼15 molecules, indicating that the two types of molecules were in a well-mixed distribution without phase separation. While dyes generally tend to exhibit a segregation structure on solid surfaces, a uniform spatial distribution was observed owing to the strong host−guest interaction caused by multiple electrostatic interaction.[15,16] In addition, the approximation of the dye structure (Pt- and Pd-TMPyP) might contribute to the realization of a uniform structure.

The number density of molecules calculated under the preparation condition at a loading level of 90% vs CEC of clay (42.4 molecules per 100 nm^2) matched well with that of the bright spots obtained from the ADF image (42.0 molecules per 100 nm^2). Further, the intensity histograms of the bright spots obtained from the ADF-STEM images of PtTMPyP (Figure S6b) and PdTMPyP (Figure S6c) show unimodal distributions. The intensity distribution can originate from the blurring of bright spots by molecular vibration, drifting of the specimen, and overlap with the contrast of clay mineral nanosheets. Although the bimodal distribution in the intensity histogram of Pt+PdTMPyP-clay (Figure S6a) partly overlap, the atomic species can be characterized accurately by separating the contrast of the clay mineral nanosheets using the intensity profile of the local region, as follows.

Figure 4f−h shows the sequential ADF-STEM images of the white-boxed region in Figure 4e from the first to the third scans. Note that the shift of the entire sample to the upper right is due to the stage drift. The stable observation of markers without any aggregation, migration, or dropout was demonstrated during the repeated scans by taking advantage of the strong fixation by multiple electrostatic interactions.[12] Also, a cleavage of the C−H bonds and subsequent cross-linking between adjacent molecules can lead to pseudostability of the heavy metal markers. We have already confirmed that there was a low possibility of cross-linking at least between the molecules using low-density molecular assembly of 20% vs CEC of clay to ensure a higher proportion of completely isolated PtTMPyP molecules, which also showed no aggregation, migration, or dropout of the bright spots.[12] It is rarely reported in most systems observed using STEM owing to the relatively weak interactions between the guest molecules and the host, such as graphene.[19,22] Figure 4i,j shows representative intensity profiles of each combination of bright spots indicated by the yellow boxed region in Figure 4f. The intensities of Pt and Pd were determined by subtracting the contrast of the clay mineral nanosheet to be 7.8×10^4 and 3.7×10^4 in Figure 4i, respectively, and 7.0×10^4 and 3.9×10^4 in Figure 4j, respectively. Similar to the intensity profile of the simulation shown in Figure 3c, the intensity ratio between Pt (brighter spots) and Pd (slightly darker spots) was approximately 2. Note that the contrast between the brighter and darker spots shows no apparent changes during repeated scans, indicating that the obtained contrast was caused by the atomic number of the marker and not by pseudoeffects such as blinking due to molecular motions. Therefore, the combination of metal atom markers of Pt ($Z = 78$) and Pd ($Z = 46$) with sufficiently different atomic numbers and ADF contrast enables the simultaneous imaging of spatial molecular distributions by ADF-STEM.

In conclusion, we succeeded in the first direct imaging of a well-mixed spatial distribution of two different types of molecules on monolayer nanosheet surfaces. The methodology presented here provides potential access to considerable local information at atomic scales, including other spatial molecular distributions and orientations. We believe that direct imaging by electron microscopy is a promising technique for the structural analysis of nonperiodic molecular assemblies constructed via weak supramolecular interactions even on relatively thick nanosheet materials and on one- to a few-atom-thick graphene analogues, thereby providing fundamental guidelines for future material design in supramolecular chemistry.

■ ASSOCIATED CONTENT

Supporting Information

The Supporting Information is available free of charge at https://pubs.acs.org/doi/10.1021/acsmeasuresciau.2c00043.

Experimental section, spectroscopic data of porphyrin-clay complexes, ADF-STEM images of Pt-, Pd-, and Zn-clay complexes, simulated ADF-STEM image of Pt+Pd-clay complex, and intensity profiles (PDF)

■ AUTHOR INFORMATION

Corresponding Authors

Yohei Ishida − *Division of Materials Science and Engineering, Faculty of Engineering, Hokkaido University, Sapporo, Hokkaido 060-8628, Japan;* orcid.org/0000-0001-8541-2714; Email: ishida-yohei@eng.hokudai.ac.jp

Tetsu Yonezawa − *Division of Materials Science and Engineering, Faculty of Engineering, Hokkaido University, Sapporo, Hokkaido 060-8628, Japan;* orcid.org/0000-0001-7371-204X; Email: tetsu@eng.hokudai.ac.jp

Author

Ikumi Akita − *Division of Materials Science and Engineering, Faculty of Engineering, Hokkaido University, Sapporo, Hokkaido 060-8628, Japan;* orcid.org/0000-0002-5843-4050

Complete contact information is available at: https://pubs.acs.org/10.1021/acsmeasuresciau.2c00043

Author Contributions

Y.I. conceived and designed the project. Y.I. and I.A. performed all experiments and analyses. T.Y. participated in the supervision of the project. I.A. wrote the manuscript using the input provided by the other authors. CRediT: **Ikumi Akita**

data curation (lead), formal analysis (lead), investigation (lead), methodology (equal), visualization (equal), writing-original draft (equal); **Yohei Ishida** conceptualization (lead), data curation (equal), formal analysis (equal), funding acquisition (lead), investigation (equal), methodology (lead), project administration (equal), resources (lead), supervision (equal), validation (equal), visualization (equal), writing-original draft (equal), writing-review & editing (lead); **Tetsu Yonezawa** conceptualization (supporting), methodology (supporting), project administration (equal), supervision (equal), validation (equal), writing-original draft (equal), writing-review & editing (equal).

Notes

The authors declare no competing financial interest.

■ ACKNOWLEDGMENTS

Y.I. acknowledges financial support from JSPS KAKENHI Grant No. 21K04805, Kurata Grant awarded by the Hitachi Global Foundation, TonenGeneral Sekiyu K.K. Foundation, The Foundation for The Promotion of Ion Engineering, Fujimori Science and Technology Foundation, The Murata Science Foundation, Takahashi Industrial and Economic Research Foundation, JACI Prize for Encouraging Young Researcher, and TEPCO Memorial Foundation Research Grant (Basic Research).

■ REFERENCES

(1) Tan, C.; Cao, X.; Wu, X. J.; He, Q.; Yang, J.; Zhang, X.; Chen, J.; Zhao, W.; Han, S.; Nam, G. H.; et al. Recent Advances in Ultrathin Two-Dimensional Nanomaterials. *Chem. Rev.* **2017**, *117*, 6225−6331.
(2) Büchner, C.; Heyde, M. Two-Dimensional Silica Opens New Perspectives. *Prog. Surf. Sci.* **2017**, *92*, 341−374.
(3) Lin, Y. C.; Susi, T.; Kotakoski, J.; Ramasse, Q. M.; Kepaptsoglou, D.; Meyer, J. C.; Suenaga, K. Towards Atomically Precise Manipulation of 2D Nanostructures in the Electron Microscope. *2D Mater.* **2017**, *4*, 042004.
(4) Sohlberg, K.; Pennycook, T. J.; Zhou, W.; Pennycook, S. J. Insights into the Physical Chemistry of Materials from Advances in HAADF-STEM. *Phys. Chem. Chem. Phys.* **2015**, *17*, 3982−4006.
(5) Nakamura, E. Atomic-Resolution Transmission Electron Microscopic Movies for Study of Organic Molecules, Assemblies, and Reactions: The First 10 Years of Development. *Acc. Chem. Res.* **2017**, *50*, 1281−1292.
(6) Lee, J. K.; Bulut, I.; Rickhaus, M.; Sheng, Y.; Li, X.; Han, G. G. D.; Briggs, G. A. D.; Anderson, H. L.; Warner, J. H. Metal Atom Markers for Imaging Epitaxial Molecular Self-Assembly on Graphene by Scanning Transmission Electron Microscopy. *ACS Nano* **2019**, *13*, 7252−7260.
(7) Bujdák, J. Effect of the Layer Charge of Clay Minerals on Optical Properties of Organic Dyes. A Review. *Appl. Clay Sci.* **2006**, *34*, 58−73.
(8) Ishida, Y. Manipulation of Precise Molecular Arrangements and Their Photochemical Properties on Inorganic Surfaces via Multiple Electrostatic Interactions. *Bull. Chem. Soc. Jpn.* **2021**, *94*, 2886−2897.
(9) Takagi, S.; Eguchi, M.; Tryk, D. A.; Inoue, H. Porphyrin Photochemistry in Inorganic/Organic Hybrid Materials: Clays, Layered Semiconductors, Nanotubes, and Mesoporous Materials. *J. Photochem. Photobiol. C Photochem. Rev.* **2006**, *7*, 104−126.
(10) Okada, T.; Ide, Y.; Ogawa, M. Organic-Inorganic Hybrids Based on Ultrathin Oxide Layers: Designed Nanostructures for Molecular Recognition. *Chem.—Asian J.* **2012**, *7*, 1980−1992.
(11) Schoonheydt, R. A.; Johnston, C. T. The Surface Properties of Clay Minerals. In *Layered Mineral Structures and their Application in Advanced Technologies*; Brigatti, M. F., Mottana, A., Eds.; Mineralogical Society of Great Britain and Ireland, 2011; Vol. *11*, pp 337−373.
(12) Akita, I.; Ishida, Y.; Yonezawa, T. Direct Imaging of Individual Organic Molecules in Supramolecular Assembly Strongly Fixed via Multivalent Electrostatic Interactions. *J. Phys. Chem. C* **2021**, *125*, 4917−4923.
(13) Yamashita, S.; Kikkawa, J.; Yanagisawa, K.; Nagai, T.; Ishizuka, K.; Kimoto, K. Atomic Number Dependence of Z Contrast in Scanning Transmission Electron Microscopy. *Sci. Rep.* **2018**, *8*, 12325.
(14) Shichi, T.; Takagi, K. Clay Minerals as Photochemical Reaction Fields. *J. Photochem. Photobiol. C Photochem. Rev.* **2000**, *1*, 113−130.
(15) Nakayama, A.; Mizuno, J.; Ohtani, Y.; Shimada, T.; Takagi, S. Elucidation of the Adsorption Distribution of Cationic Porphyrin on the Inorganic Surface by Energy Transfer as a Molecular Ruler. *J. Phys. Chem. C* **2018**, *122*, 4365−4371.
(16) Ghosh, P. K.; Bard, A. J. Photochemistry of Tris(2,2′-Bipyridyl)Ruthenium(II) in Colloidal Clay Suspensions. *J. Phys. Chem.* **1984**, *88*, 5519−5526.
(17) Akita, I.; Ishida, Y.; Yonezawa, T. Atomic-Scale Imaging of a Free-Standing Monolayer Clay Mineral Nanosheet Using Scanning Transmission Electron Microscopy. *J. Phys. Chem. Lett.* **2020**, *11*, 3357−3361.
(18) Mittelberger, A.; Kramberger, C.; Meyer, J. C. Insights into Radiation Damage from Atomic Resolution Scanning Transmission Electron Microscopy Imaging of Mono-Layer $CuPcCl_{16}$ Films on Graphene. *Sci. Rep.* **2018**, *8*, 4813.
(19) Sinha, S.; Warner, J. H. Recent Progress in Using Graphene as an Ultrathin Transparent Support for Transmission Electron Microscopy. *Small Struct.* **2021**, *2*, 2000049.
(20) Gerkman, M. A.; Sinha, S.; Warner, J. H.; Han, G. G. D. Direct Imaging of Photoswitching Molecular Conformations Using Individual Metal Atom Markers. *ACS Nano* **2019**, *13*, 87−96.
(21) Koshiya, S.; Yamashita, S.; Kimoto, K. Microscopic Observation of Dye Molecules for Solar Cells on a Titania Surface. *Sci. Rep.* **2016**, *6*, 24616.
(22) Kengmana, E. S.; Lee, J. K.; Li, X.; Warner, J. H.; Han, G. G. D. Self-Assembly of Bowlic Supramolecules on Graphene Imaged at the Individual Molecular Level Using Heavy Atom Tagging. *Small* **2020**, *16*, 2002860.
(23) Gerkman, M. A.; Lee, J. K.; Li, X.; Zhang, Q.; Windley, M.; Fonseca, M. V.; Lu, Y.; Warner, J. H.; Han, G. G. D. Direct Imaging of Individual Molecular Binding to Clean Nanopore Edges in 2D Monolayer MoS_2. *ACS Nano* **2020**, *14*, 153−165.

https://doi.org/10.1021/acsmeasuresciau.2c00043
ACS Meas. Sci. Au 2022, 2, 542−546